

## Bifurcations of dividing surfaces in chemical reactions

Manuel Iñarraea,<sup>1,a)</sup> Jesús F. Palacián,<sup>2</sup> Ana Isabel Pascual,<sup>3</sup> and J. Pablo Salas<sup>1,b)</sup>

<sup>1</sup>Área de Física Aplicada, Universidad de La Rioja, Logroño, Spain

<sup>2</sup>Departamento de Ingeniería Matemática e Informática, Universidad Pública de Navarra, Pamplona, Spain

<sup>3</sup>Departamento de Matemáticas y Computación, Universidad de La Rioja, Logroño, Spain

(Received 9 March 2011; accepted 26 May 2011; published online 7 July 2011)

We study the dynamical behavior of the unstable periodic orbit (NHIM) associated to the non-return transition state (TS) of the  $H_2 + H$  collinear exchange reaction and their effects on the reaction probability. By means of the normal form of the Hamiltonian in the vicinity of the phase space saddle point, we obtain explicit expressions of the dynamical structures that rule the reaction. Taking advantage of the straightforward identification of the TS in normal form coordinates, we calculate the reaction probability as a function of the system energy in a more efficient way than the standard Monte Carlo method. The reaction probability values computed by both methods are not in agreement for high energies. We study by numerical continuation the bifurcations experienced by the NHIM as the energy increases. We find that the occurrence of new periodic orbits emanated from these bifurcations prevents the existence of a unique non-return TS, so that for high energies, the transition state theory cannot be longer applied to calculate the reaction probability. © 2011 American Institute of Physics. [doi:10.1063/1.3600744]

### I. INTRODUCTION

Since the decade of 1930s, transition state theory (TST) has been a fundamental tool in the study of chemical reaction dynamics.<sup>1</sup> Assuming that in a chemical reaction reactant and product regions are kept apart by a *barrier*, the main assumption of the TST relies on the existence of a dividing surface located at the neighborhood of the barrier, the so-called transition state (TS), that separates reactants from products. A proper TS presents two properties: it is only crossed by reactive trajectories, and it is a non-recrossing surface in the sense that reactive trajectories must cross it only once. Because the reaction rate is proportional to the directional flux through the TS,<sup>2–5</sup> if any of these conditions does not hold, the TST would lead to an overestimation of the reaction rate.

For a two degrees of freedom (2 DOF) reaction (for instance a collinear triatomic exchange reaction) whose Hamiltonian is expressed as kinetic plus potential energies, it is well known from the 1970s that the projection in the configuration space of an unstable periodic orbit living in the vicinity of the saddle point (the so-called Lyapunov orbit) plays the role of dividing surface (TS).<sup>2–7</sup> For a given energy, this projection is a line that bridges the corresponding equipotential curves and it keeps the reactant and the product regions apart.

However, for 2 DOF chemical reactions whose Hamiltonians are no longer in the form kinetic plus potential or for chemical reactions of higher dimension, the above picture defined in the configuration space breaks (see Ref. 8 for a short and clear review of this subject). Then, the

general question of how to construct the TS for arbitrary  $n$  DOF chemical reactions remained unsolved during decades. Recently, when the barrier between reactants and products corresponds to an index one critical point (*saddle point*) in the Hamiltonian of the reaction, the answer to this question came from the hand of nonlinear dynamics. Indeed, in the 1990s Wiggins<sup>9</sup> showed that a normally hyperbolic invariant manifold (NHIM) is associated with the phase space geometry in the vicinity of the saddle point. With this result and using Poincaré–Birkhoff theory,<sup>10</sup> in the early 2000s it was possible to obtain analytically the dividing surface (e.g., the TS) that separates reactants from products with the required non-return property. Furthermore, when the Hamiltonian is in normal form, all the geometrical objects that in phase space define the TS appear in a natural way. Note that now phase space is the playground for the development of this new transition state theory. For a review of the subject, we refer the reader to Refs. 11 and 12. Under this new formulation, the TST has also been successfully applied in different fields as atomic physics<sup>13</sup> or celestial mechanics.<sup>14</sup>

In this geometrical formulation of the TST, the NHIM, which is a (invariant) manifold of dimension  $(2n - 3)$  living in the neighborhood of the saddle, is of fundamental importance. We note that for 2 DOF, the NHIM reduces to the Lyapunov periodic orbit, which allowed Pollak and co-workers to define the aforementioned dividing surfaces in the configuration space.

Furthermore, the validity of this integrable model depends on that the NHIM preserves the no-return property. The non-return property is closely linked to the phase space has the “bottleneck” structure.<sup>3,5,15–17</sup> That is to say, with the existence of a small region in phase space that separates two large regions. In the case of chemical reactions, the large phase space regions are the reactants and the

<sup>a)</sup>Electronic mail: manuel.inarraea@unirioja.es.

<sup>b)</sup>Electronic mail: josepablo.salas@unirioja.es.

products, while the bottleneck corresponds to the phase space region around the barrier, e.g., the saddle point. Whether or not the phase space presents the bottleneck property depends on the value of the energy. For energy values below the saddle point energy, the reactant and product regions are disjoint regions and (classically) no reactive trajectories are allowed. At low energies above the barrier, we find the bottleneck property because the energy shell in the neighborhood of the saddle is very narrow. However, as the energy increases, the bottleneck property is lost because there is a wide available phase space region around the saddle point and, roughly speaking, it makes no sense to talk about reactants and products.

When the systems bears the bottleneck property, the TST is exact and it is possible to find a unique dividing surface (TS) around the saddle point region. In this situation, the NHIM bounds the TS, only reactive trajectories cross the TS, they do it once, and the reaction rate is proportional to the flux across the NHIM. However, as the energy increases, the bottleneck (non-return) property of the system is lost and both reactive and non-reactive trajectories may cross the TS many times. In this situation, when the flux across the NHIM is evaluated, one gets an overestimation of the reaction rate. It is important to realize that the root of this behavior is completely dynamical in the sense that there is not any structural change in the neighborhood of the saddle region.

The loss of the bottleneck property for 2 DOF has been detected and studied since 1970s by several authors. For the collinear  $\text{H}_2 + \text{H}$  exchange reaction, Pechukas and co-workers<sup>2-5,7</sup> were the first to realize that no-return property depends on the existence of a unique dynamical barrier around the saddle. They found that, from a certain energy above the saddle, there appeared additional periodic orbits away from the saddle acting as new dynamical barriers that caused the overestimation of the reaction rate. Following these works and for the same chemical reaction, Grimmelmann and Lohr<sup>18</sup> and Sverdlik and Koeppl<sup>19</sup> investigated the exactness and the validity of the TST. However, all these works were done in the configuration space while the dynamics actually takes place in phase space. In this sense and again for 2 DOF chemical reactions, Davis<sup>15-17</sup> was one of the first to address the breakdown of the TST from the phase space point of view.

Later on, for the collinear reaction  $\text{HgI}_2 \rightarrow \text{HgI} + \text{I}$ , Burghardt and Gaspard<sup>20</sup> showed numerically that, as the energy increases, they appear new periodic orbits due to bifurcations in the saddle point region. These authors noted that this fact ruins the no-return property provided by the original NHIM and, in consequence, the breakdown of the TST.

Recently, Li *et al.*<sup>21,22</sup> studied analytically the definability of no-return transition states in the high energy regime by using “partial” normal forms. In particular, taking the energy of the system as the bifurcation parameter, these authors applied this technique to the collinear  $\text{H}_2 + \text{H}$  exchange reaction to study the bifurcations of the the primary NHIM. Moreover, they obtained relevant information about the topological changes of phase space in the saddle point region. These changes, closely related to Davis’ results,<sup>17</sup> together with the bifurcation diagram, allowed them to identify the new unsta-

ble periodic orbit with respect to which the no-return TS is defined.<sup>22</sup>

Taking the  $\text{H}_2 + \text{H}$  collinear reaction as an example, this paper is devoted to get a deeper insight into the central role played by bifurcations in the loss of the bottleneck property and the breakdown of TST. For this, we will continue numerically the main families of periodic orbits that bifurcate from the original NHIM of the system. The NHIM is determined through the normal form Hamiltonian. Then, using the NHIM, we calculate the evolution of the reaction probability as a function of the energy, and we compare these results to those obtained by a Monte Carlo method. Up to a certain energy, the significant deviations found will allow us to put into question the existence of a unique no-return TS and the breakdown of the TST.

The paper is organized as follows. In Sec. II we give an overview on the transition state theory that permit the analytical construction of a no-return transition state. In Sec. III we apply this theory to the collinear  $\text{H}_2 + \text{H}$  reaction and we determine the geometric structures that govern the reaction. In Sec. IV we use the results of the previous one to determine the reaction probability as a function of the energy. A comparison to the results obtained with Monte Carlo calculations is also done. In Sec. V we study the bifurcations of the NHIM. Section VI is devoted to the discussion of the breakdown of the TST. Finally, in Sec. VII we summarize the results.

## II. AN OVERVIEW OF THE CONSTRUCTION OF A NON-RETURN TRANSITION STATE

We consider an arbitrary  $n$ -degrees of freedom Hamiltonian  $\mathcal{H}(x_1, \dots, x_n, p_{x_1}, \dots, p_{x_n})$  which has an index one equilibrium point (saddle point)  $P_s$  of energy  $E_s$ . Without loss of generality, we assume that  $P_s$  is located at the origin. The eigenvalues of the matrix associated to the linearized Hamiltonian equations of motion around  $P_s$  are of the form:

$$\pm\omega_n, \quad \pm i \omega_j, \quad j = 1, \dots, n-1.$$

The real eigenvalues  $\pm\omega_n$  describe the hyperbolic direction of the saddle point (i.e., the reactive direction) while the  $n-1$  complex pairs of eigenvalues stand for the  $n-1$  elliptic directions of the saddle point (i.e., the non-reactive or “bath” modes). In the neighborhood of the saddle point, the phase space geometry becomes transparent when  $\mathcal{H}$  is transformed into its normal form. The procedure is carried into two main steps. In the first one, we express  $\mathcal{H}$  as an  $N$  degree Taylor expansion around  $P_s$  in the following way:

$$\mathcal{H} \approx E_s + \sum_{i=1}^{n-1} \frac{1}{2} (p_{x_i}^2 + \omega_i^2 x_i^2) + \frac{1}{2} (p_{x_n}^2 - \omega_n^2 x_n^2) + \sum_{j=3}^N \mathcal{H}_j, \quad (1)$$

where  $\mathcal{H}_j$  are the terms of the expansion of degree  $j \geq 3$ . Then, using the Poincaré–Birkhoff normalization technique, we construct a sequence of local canonical nonlinear transformations that express (1) into its normal form  $\mathcal{K}$  up to the desired degree  $N$ :

$$\mathcal{H}(x_1, \dots, x_n, p_{x_1}, \dots, p_{x_n}) \longrightarrow \mathcal{K}(q_1, \dots, q_n, p_1, \dots, p_n).$$

When in normal form, the Hamiltonian  $\mathcal{K}$  reads as

$$\mathcal{K} = E_s + \sum_{i=1}^{n-1} J_i + \mathcal{I} + \mathcal{F}(J_1, \dots, J_{n-1}, \mathcal{I}), \quad (2)$$

where  $\mathcal{I} = (p_n^2 - \omega_n^2 q_n^2)/2$  and  $J_i = (p_i^2 + \omega_i^2 q_i^2)/2$ ,  $i = 1, \dots, n-1$  are the canonical actions of the system. The term  $\mathcal{F}$  is made of polynomials in  $(J_1, \dots, J_n, \mathcal{I})$  of degree  $j$  with  $2 \leq j \leq N/2$  and it is responsible for the nonlinear terms. Note that this result is valid in the neighborhood of the saddle point. For a revision of the procedure see Ref. 10 and references therein. From a mathematical point of view, the key feature of this technique is that the Hamiltonian  $\mathcal{K}$  is expressed solely as a function of the new  $n$  integrals  $(J_1, \dots, J_{n-1}, \mathcal{I})$ . From a chemical point of view, with this procedure the local separability between the reactive degree of freedom  $\mathcal{I}$  and the  $n-1$  non-reactive degrees of freedom  $J_i$  is achieved. Around the saddle point the dynamics takes place in the  $(2n-1)$ -dimensional energy surface given by  $\mathcal{K}$ . The corresponding Hamilton equations of motion take the following form:

$$\begin{aligned} \dot{q}_i &= \frac{\partial \mathcal{K}}{\partial J_i}(J_1, \dots, J_{n-1}, \mathcal{I}) p_i, & i = 1, \dots, n-1, \\ \dot{p}_i &= -\frac{\partial \mathcal{K}}{\partial J_i}(J_1, \dots, J_{n-1}, \mathcal{I}) q_i, & i = 1, \dots, n-1, \\ \dot{q}_n &= \frac{\partial \mathcal{K}}{\partial \mathcal{I}}(J_1, \dots, J_{n-1}, \mathcal{I}) p_n, \\ \dot{p}_n &= \frac{\partial \mathcal{K}}{\partial \mathcal{I}}(J_1, \dots, J_{n-1}, \mathcal{I}) q_n. \end{aligned} \quad (3)$$

From (3) it is clear that  $q_n = p_n = 0$  is a  $(2n-3)$ -dimensional invariant manifold. Moreover, it is a normally hyperbolic invariant manifold.<sup>9</sup> Normal hyperbolicity means that the expansions and contractions normal to the manifold dominate those tangents to it. Basically, the NHIM is a higher-dimensional saddle point. Therefore, the NHIM has attached stable  $\mathcal{W}^s$  and unstable  $\mathcal{W}^u$  manifolds which act like multidimensional separatrices. These surfaces are  $(2n-2)$ -dimensional spherical cylinders given by setting, respectively,  $p_n = -q_n$  and  $p_n = q_n$  in  $\mathcal{K}$ . Note that  $\mathcal{W}^s$  and  $\mathcal{W}^u$  have the right dimension to divide the phase space and, thence they are impenetrable barriers in phase space<sup>12</sup> that separate reactive from non-reactive trajectories.

The NHIM is the limit (“equator”) of a  $(2n-2)$ -dimensional sphere obtained by setting  $q_n = 0$  in  $\mathcal{K}$ . This  $(2n-2)$ -dimensional sphere  $D_{TS}$  is the TS. The TS is locally a surface of no-return because it is transverse to the Hamiltonian flow: when a trajectory crosses the TS, it must leave it before (possible) re-intersects the TS.<sup>11,12,23</sup> The NHIM divides the TS into two hemispheres  $D_{TS}^f$  and  $D_{TS}^b$  with  $p_n > 0$  and  $p_n < 0$ , respectively. The halve  $D_{TS}^f$  ( $D_{TS}^b$ ) is always crossed by forward (backward) reactive trajectories.

Hence,  $\mathcal{W}^{s,u}$  bound a region in the  $(2n-1)$ -dimensional energy surface  $\mathcal{K}$  that is divided into two components by the TS. All reactive trajectories start in one component, cross the TS and enter the other component.

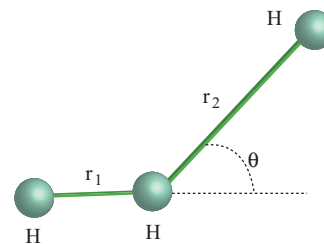


FIG. 1. Coordinates of the  $\text{H}_2 + \text{H}$  exchange reaction.

### III. THE COLLINEAR $\text{H}_2 + \text{H}$ REACTION

Now we apply the theory outlined in Sec. II to the  $\text{H}_2 + \text{H}$  exchange reaction. For zero total angular momentum, the classical three-degrees of freedom Hamiltonian describing this reaction is given by

$$\begin{aligned} \mathcal{H} &= \frac{p_{r_1}^2 + p_{r_2}^2 - p_{r_1} p_{r_2} \cos \theta}{m_H} + \frac{p_\theta \sin \theta}{m_H} \left( \frac{p_{r_1}}{r_1} + \frac{p_{r_2}}{r_2} \right) \\ &+ \frac{p_\theta^2}{m_H} \left( \frac{1}{r_1^2} + \frac{1}{r_2^2} + \frac{\cos \theta}{r_1 r_2} \right) + V(r_1, r_2, \theta), \end{aligned} \quad (4)$$

where  $m_H$  is the hydrogen mass,  $(r_1, r_2)$  are the two relative distances between the three hydrogen atoms and  $\theta$  is the bending angle (see Fig. 1). The term  $V(r_1, r_2, \theta)$  is the potential energy surface (PES) governing the dynamics of the reaction. Throughout the paper atomic units are used. Because the  $\text{H}_2 + \text{H}$  reaction is a paradigm in chemical reaction dynamics, there are several options in the choice of  $V(r_1, r_2, \theta)$ . In this work we use two different models: the classical Porter–Karplus (PK) energy surface<sup>24</sup> and the more modern and accurate energy surface by Boothroyd, Keogh, Martin, and Peterson (BKMP).<sup>25</sup> Although at slightly different positions and energy values, both surfaces present a unique critical point, namely a saddle point at  $r_{1s} = r_{2s} = r_s$  in the collinear direction  $\theta = 0$  (see Fig. 2 and Table I).

It is easy to check in the equations of motion arising from Eq. (4) that the phase point made of the critical point  $r_{1s} = r_{2s} = r_s$  in the collinear direction ( $\theta = 0$  or  $\theta = \pi$ ), together with the conditions  $p_{r_1} = p_{r_2} = p_\theta = 0$ , is a saddle point of the Hamiltonian flow. Moreover, if we consider initial conditions along the collinear direction ( $\theta = p_\theta = 0$ ), we get  $\dot{\theta} = \dot{p}_\theta = 0$ , meaning that the collinear direction is invariant under the Hamiltonian flow. Then, we reduce out this direction in order to manage a two degrees of freedom Hamiltonian system.

We apply the transition state theory in the collinear case as follows. First, by means of a linear change in Hamiltonian (4), we move the saddle point to the origin. After the translation, we prepare the resulting Hamiltonian for its transformation into normal form. Indeed, we express the Hamiltonian in the form given by Eq. (1) by performing a Taylor expansion around the origin (i.e.,  $P_s$ ). Using the symbolic manipulator *MATHEMATICA*, we compute the normal form  $\mathcal{K}$  of the expanded Hamiltonian up to degree  $N = 14$  and drop higher degree terms. At this point it is important to understand that  $\mathcal{K}$  is expressed as a function of the normal form coordinates denoted as  $(q_1, q_2, p_1, p_2)$  and that  $\mathcal{K}$

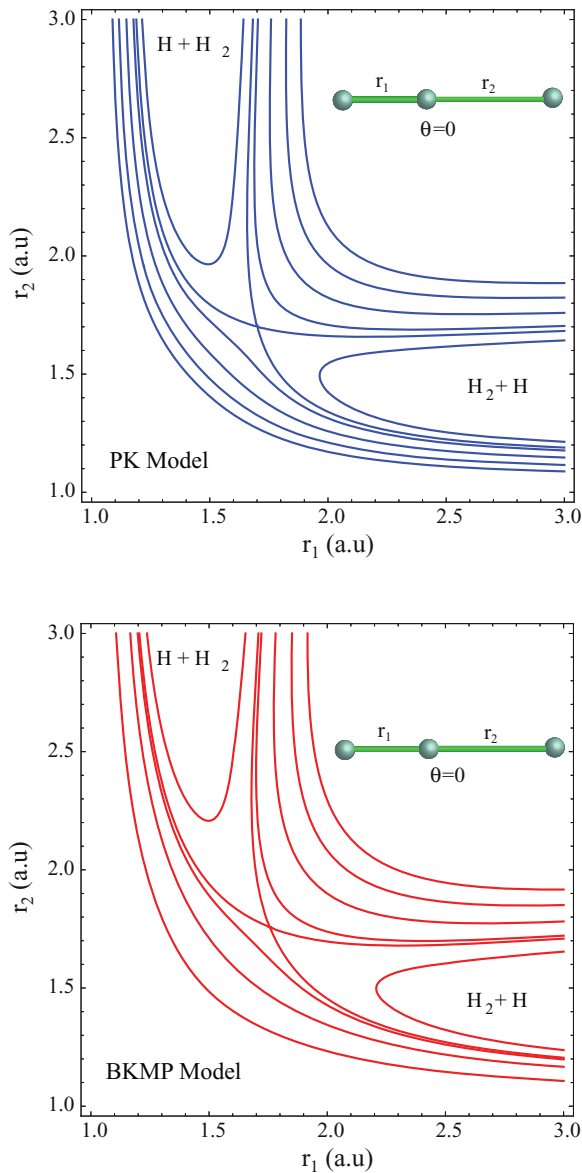


FIG. 2. Equipotential curves of the PK and BKMP potential energy surfaces of the collinear  $\text{H}_2 + \text{H}$  exchange reaction. In both figures, besides the saddle point energy equipotential, they are represented the equipotential curves corresponding to the energies of 0.014, 0.016, 0.020, 0.025, and 0.030 a.u.

is integrable because the quantities  $J = (p_1^2 + \omega_1^2 q_1^2)/2$  and  $\mathcal{I} = (p_2^2 - \omega_2^2 q_2^2)/2$  are the new (approximate) integrals. Then, the normal form is expressed as

$$\mathcal{K} = \mathcal{K}(J, \mathcal{I}) = E_s + J + \mathcal{I} + \sum_{i=2}^N \mathcal{K}_i(J, \mathcal{I}), \quad (5)$$

where  $\mathcal{K}_i$  are homogeneous polynomials of degree  $i/2 \geq 2$  in  $J$  and  $\mathcal{I}$ . Once the normal form is computed, we obtain

TABLE I. Properties of the saddle point of the PK and BKMP potential energy surface models. All values are in a.u.

PES model	Saddle position ( $r_{1s} = r_{2s}$ )	Energy $E_s$ of the saddle
PK	1.70083	0.014557
BKMP	1.75700	0.015203

the NHIM, the TS,  $\mathcal{W}^s$ , and  $\mathcal{W}^u$  by setting in  $\mathcal{K}$ , respectively,  $q_2 = p_2 = 0$ ,  $q_2 = 0$ ,  $p_2 = -q_2$ , and  $p_2 = q_2$ .

Due to the fact that the normal form provides the direct and inverse transformations between the normal form coordinates and the original coordinates, we have the expressions of the original coordinates ( $r_1, r_2, p_{r_1}, p_{r_2}$ ) as a function of the normal form coordinates ( $q_1, q_2, p_1, p_2$ ). By introducing in these (inverse) transformations the above conditions  $q_2 = p_2 = 0$ ,  $q_2 = 0$ ,  $p_2 = -q_2$ , and  $p_2 = q_2$ , we have the parametric expressions of all the mentioned manifolds in the original coordinates. These expressions can be used, among other things, to visualize these structures. In particular, using the BKMP energy surface and the normal form calculated for an energy  $\mathcal{H} = E = 0.016$  a.u., projections in the original coordinates of the four structures are shown in Fig. 3. We note that, because our system has two degrees of freedom, the NHIM is an unstable periodic orbit whose projection onto the configuration space bridges the corresponding equipotential curves  $V(r_1, r_2, \theta = 0) = 0.016$  a.u. (see Fig. 3). In fact, due to the symmetry of the reaction, this projection is the bisector  $r_1 = r_2$  of the  $(r_1, r_2)$  plane.

#### IV. PHASE FLUX AND REACTION PROBABILITY

Usually, the calculation of the reaction probability of a given chemical reaction is carried out by using expensive brute force Monte Carlo methods. However, the theory outlined in Sec. II provides a “cheaper” method to calculate this quantity. It was shown in Refs. 2 and 8 that, for a given energy  $E$ , the reaction probability  $P(E)$  can be calculated as the fraction

$$P(E) = \frac{\Phi_{TS}}{\Phi_{Total}},$$

where  $\Phi_{TS}$  is the reactive phase flux crossing the transition state, and  $\Phi_{Total}$  is the total incident phase flux. When the Hamiltonian of the system is in normal form  $\mathcal{K}$ , the  $\Phi_{TS}$  is given by the flux crossing the forward dividing surface  $D_{TS}^f$  and it is obtained by means of the integral<sup>8,26</sup>

$$\Phi_{TS} = \int_{D_{TS}^f} \Omega, \quad \text{with} \\ \Omega = dq_1 \wedge dp_1 + \dots + dq_{n-1} \wedge dp_{n-1}$$

where  $(q_1, \dots, q_n, p_1, \dots, p_n)$  are the normal form coordinates. Taking into account that  $D_{TS}^f$  is limited by the NHIM, and making use of the Stokes theorem, the flux  $\Phi_{TS}$  can be directly computed as the action over the NHIM, namely,

$$\Phi_{TS} = \oint_{\text{NHIM}} p_1 dq_1 + \dots + p_{n-1} dq_{n-1} = (2\pi)^{n-1} \mathcal{S},$$

where  $\mathcal{S}$  is the “area” enclosed by the contour  $\mathcal{K}_{\text{NHIM}} = \mathcal{K}(J_1, \dots, J_{n-1}, 0) = E$ . Note that the proper geometric object that controls the reaction (the dividing surface) is not the  $(2n - 2)$ -dimensional sphere  $D_{TS}$  but the NHIM. In fact, the definition of the TS (the sphere  $D_{TS}$ ) is not unique.<sup>23</sup>

In our collinear reaction,  $\Phi_{TS}$  is readily obtained from the normal form (5) by solving the equation  $\mathcal{K}(J, 0) = E$ .

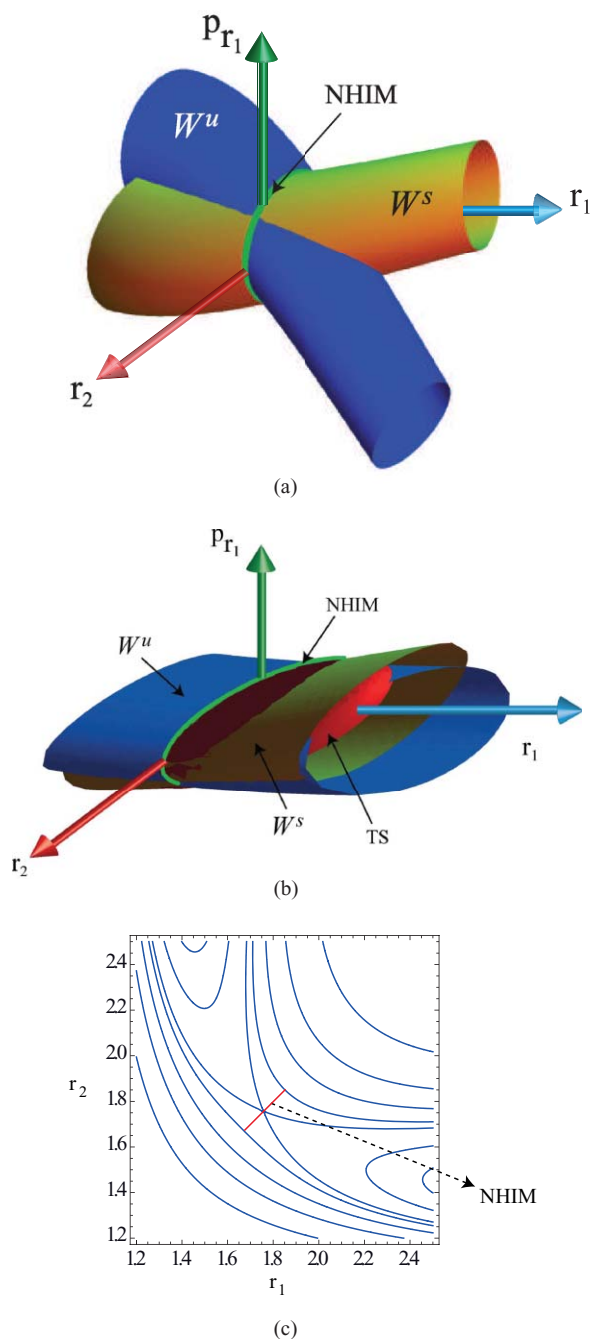


FIG. 3. Projections in the original coordinates of the NHIM, the TS, and the stable and unstable manifolds  $W^s$  and  $W^u$  for an energy  $E = 0.016$  a.u.

To compute the total flux  $\Phi_{Total}$ , we assume that one of the hydrogen atoms is infinitely away ( $r_2 \rightarrow \infty$ ) from the  $H_2$  molecule. Thence, the PES does not depend on  $r_2$  because it is essentially the potential energy curve of the  $H_2$  diatomic target. Then, for a given energy  $E$ , the total flux  $\Phi_{Total}$  is the flux across the two-dimensional (forward) surface  $\mathcal{D}_f$ :

$$\mathcal{D}_f \equiv E = \frac{p_1^2 + p_2^2 - p_1 p_2}{m_H} + V(r_1, r_2 \rightarrow \infty, \theta = 0). \quad (6)$$

Because the domain  $\mathcal{D}_f$  is limited by the closed curve  $\mathcal{C}_f$ ,

$$\mathcal{C}_f \equiv E = \frac{p_1^2 + p_2^2 - p_1 p_2}{m_H} + V(r_1 = r_{min}, r_2 \rightarrow \infty, \theta = 0), \quad (7)$$

where  $r_{min}$  is the equilibrium distance of the  $H_2$  diatomic, we use again the Stokes theorem to compute the total flux  $\Phi_{Total}$  as the action over  $\mathcal{C}_f$ .

The initial conditions  $(r_1^o, r_2^o, p_1^o, p_2^o)$  of the trajectories for the Monte Carlo calculations are taken by considering that  $r_2^o \rightarrow \infty$  and  $\dot{r}_2^o < 0$ . In our calculations we take  $r_2^o = 50$  a.u. As we said, under the condition  $r_2^o \rightarrow \infty$ , the potential energy surface does not depend on the value of  $r_2$ . Then, if  $E$  is the total energy of the system, the available values of  $r_1^o$  must hold the condition

$$E > V(r_1^o, r_2^o \rightarrow \infty, \theta = 0).$$

For each value of  $r_1^o$  satisfying the above condition, the possible values of  $(p_1^o, p_2^o)$  are within the domain (7) with  $\dot{r}_2^o < 0$ .

The integration of a given trajectory stops when: (a) the  $r_1$  coordinate crosses with  $\dot{r}_1 > 0$  the threshold value of 50 a.u. (e.g.,  $r_1 \rightarrow \infty$ ) while  $r_2$  remains bounded; or (b) coordinate  $r_2$  reaches again the initial value  $r_2^o = 50$  a.u. with  $\dot{r}_2^o > 0$  and with bounded  $r_1$ . In the first case the trajectory is taken to be reactive, while in the second one it is considered as non-reactive. These criteria do not include dissociation trajectories because in the considered energy range, these outcomes are not allowed.

For comparison, Fig. 4 shows the evolution with the energy  $E$  of the reaction probabilities calculated with both methods. The probability  $P_{NF}(E)$  computed with the method involving the normal form, and the probability  $P_{MC}(E)$  calculated by the standard trajectory Monte Carlo method. Figure 4(a) corresponds to the reaction described by the BKMP potential energy surface, whereas Fig. 4(b) stands for the reaction portrayed by the PK potential energy surface.

From this figure, it is clear that for both potential energy surfaces and for energies up to  $E \approx 0.22$  a.u., the probability values calculated with both methods are in very good agreement. Therefore, in these conditions it is correct to consider  $D_{TS}$  as the unique dividing surface that separates reactants from products and that controls the reaction. Nevertheless, for energies  $E > 0.22$  a.u., the probability calculated with the normal form  $P_{NF}(E)$  presents a wrong monotonic increase instead of the predicted falloff for high energies.<sup>2,5</sup>

## V. BIFURCATIONS OF THE NHIM

The results of Sec. IV indicate that for energies high enough, the unstable periodic orbit given by the NHIM cannot be longer regarded as the dividing surface that rules the reaction. In this respect, several authors<sup>2,20–22</sup> have related this fact to bifurcation phenomena suffered by the NHIM at high energies. Then, we focus on the numerical detection of possible bifurcations of the NHIM as the system energy increases. This study also allows us to identify the new families of periodic orbits emanating from the NHIM.

With this in mind, and taking the energy  $E$  as the parameter, we make the bifurcation analysis of the original NHIM

by means of the numerical continuation of the families of periodic orbits emanating from it. We performed this study for both potential energy surfaces. This numerical analysis is carried out using the freely distributed software package AUTO2007.<sup>27–29</sup>

In the case of the PK potential energy surface, Fig. 5 shows the bifurcation diagram of the different families of periodic orbits connected to the original NHIM (family  $F_0$ ) for increasing energy  $E$ . The goal of this figure is to show in the clearest way the sequence of bifurcations experienced by the NHIM as the energy  $E$  increases and the different families of periodic motions emanated from the NHIM. Therefore, for the sake of clarity, the vertical axis of this figure does not represent any quantitative magnitude or norm related to the periodic solutions, that would result in a more confusing and obscure bifurcation diagram. This also stands for Fig. 7. In fact, the complete bifurcation diagram is made of this one and its mirror reflection with respect to the energy axis, but for the sake of simplicity, in the figure it is only represented one half. The first two bifurcations of the system are of saddle-node type, and they occur symmetrically at both sides of the saddle point for an energy  $E \approx 0.022$  a.u. (see Fig. 5). From these bifurcations two new families of periodic orbits arise (one stable  $F_2$  and the other unstable  $F_1$ , depicted by two blue lines in the diagram). These new families, which correspond to off-diagonal asymmetric stretching motions (that is, periodic orbits whose projection on the configuration space is out

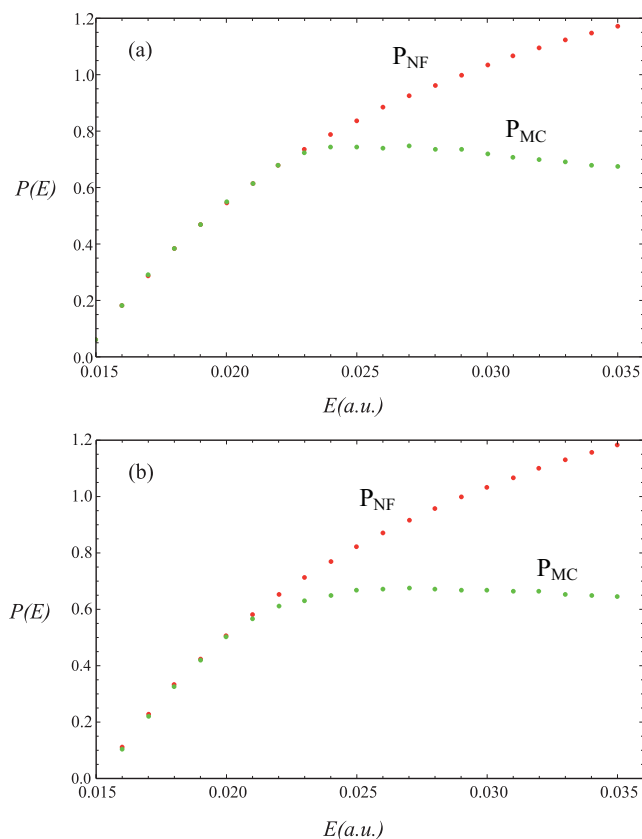


FIG. 4. Evolution of the reaction probabilities with the system energy  $E$  computed by the standard Monte Carlo method (green points) and by the method involving the normal form (red points). (a) PK potential energy surface; (b) BKMP potential energy surface.

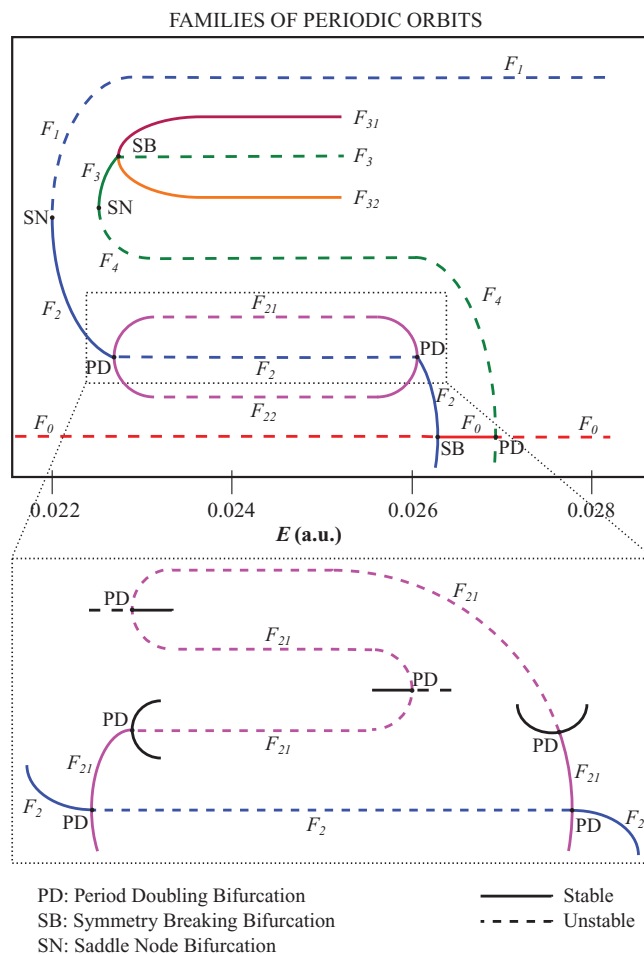


FIG. 5. Bifurcation diagram of the families of periodic orbits connected to the original NHIM ( $F_0$ ) for increasing energies  $E$  in the case of the PK potential energy surface.

of the  $r_1 = r_2$  diagonal), have already been reported by several authors.<sup>2,5,22</sup> Figure 6(a) shows the projections of these periodic orbits and the original NHIM on the  $(r_1, r_2)$  plane as well as the equipotential energy lines. As the energy of the system increases, the two unstable periodic orbits  $F_1$  (the dashed blue line) migrate away from the saddle point without undergoing any further bifurcation. On the other hand, the two stable periodic orbits  $F_2$  (the solid blue line) approach the saddle point with increasing energy, and finally they collapse with the original NHIM (the red line) in a symmetry breaking bifurcation for an energy  $E \approx 0.02654$  a.u. In this bifurcation scenario, the family  $F_0$  becomes stable for a short interval of increasing energy.

In the migration of  $F_2$  (the blue line) toward the saddle point, it undergoes a period-doubling bifurcation for  $E \approx 0.02207$  a.u., from which two new families of periodic orbits appear (magenta lines  $F_{21}$  and  $F_{22}$ ). These new periodic motions are the unfolding of the parent  $F_2$ . In this sense, the shapes of their projections in the  $(r_1, r_2)$  plane resemble two deformed bells, see Fig. 6(b). These new periodic motions have a transient existence with increasing energy, although they experience a quite complicated evolution, depicted in the inset of Fig. 5, with a chain of consecutive period-doubling bifurcations. Finally, these families collapse again with

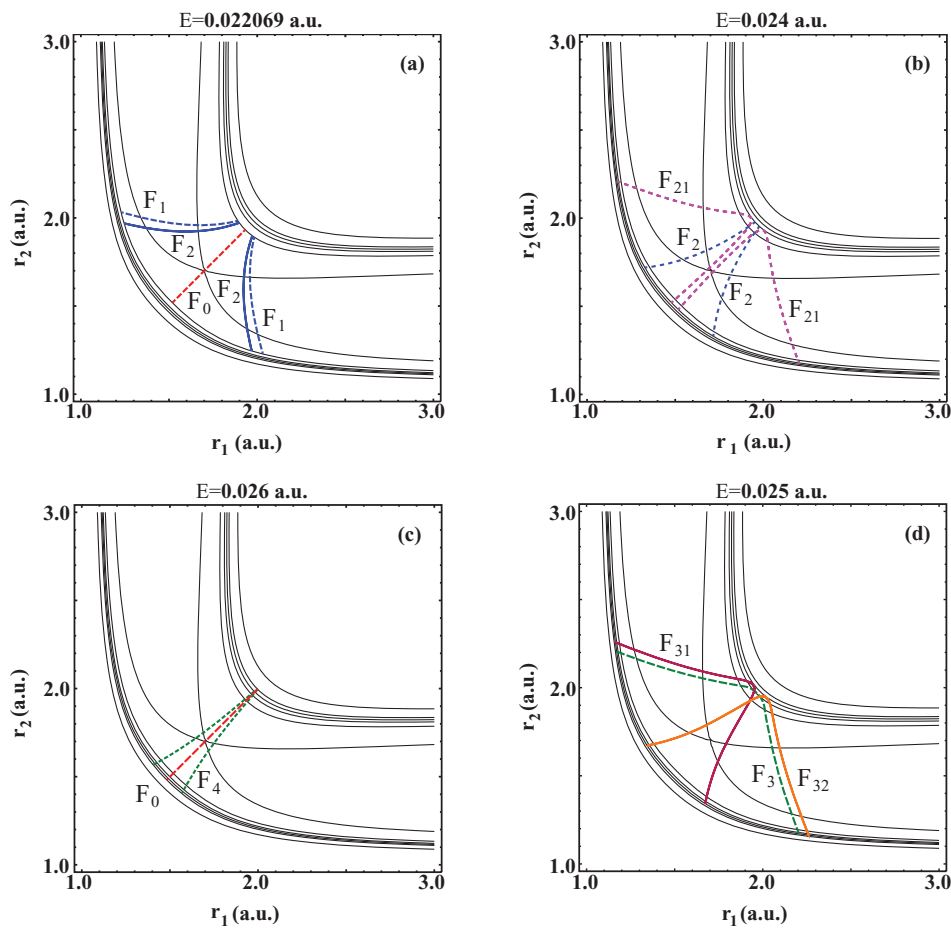


FIG. 6. Projections on the  $(r_1, r_2)$  plane of the different periodic motions involved in the bifurcations diagram of Fig. 5. Besides the equipotential curves corresponding to the energies of the four panels, they are also plotted the equipotential lines of the saddle point energy and the energy  $E = 0.03$  a.u.

the  $F_2$  family (the blue line) in an inverse period-doubling bifurcation for  $E \approx 0.02651$  a.u.

Coming back to the evolution of the original NHIM (family  $F_0$ , red line), it suffers a second bifurcation for  $E \approx 0.02661$  a.u. This is a period-doubling bifurcation in which two new families of unstable periodic orbits emerge (the green line  $F_4$ ). The projection of these new unstable motions on the  $(r_1, r_2)$  plane has a bell shape symmetric with respect to the diagonal, see Fig. 6(c), as it arises from the unfolding of the symmetric stretching  $F_0$ . This new family of unstable periodic motions evolves for decreasing energy, and its bell shape gets wider as the energy decreases. The origin of this family is in a saddle-nodde bifurcation that occurs for an energy  $E \approx 0.02254$  a.u. In fact, two families of bell-shaped periodic motions come up from this saddle-nodde bifurcation. One of them is the unstable family  $F_4$  that collapses with  $F_0$ , while the other family  $F_3$  corresponds to stable bell shaped motions that gets wider as the energy increases. For an energy  $E \approx 0.022561$  a.u., this family undergoes a symmetry breaking bifurcation in which it becomes unstable and two new families of stable periodic motions appear (the orange and brown lines  $F_{32}$  and  $F_{31}$ ). Figure 6(d) shows the projection of these new stable motions on the  $(r_1, r_2)$  plane.

Figure 7 shows the bifurcation diagram of the families of periodic orbits connected to the original NHIM for increasing

energy  $E$  in the case of the BKMP potential energy surface. This bifurcation diagram is completely different from the previous one corresponding to the PK potential energy surface. In this case, the new families of periodic orbits emanate from the original NHIM (family  $F_0$ ) in a more ordered sequence of bifurcations as the system energy increases. Besides, this sequence of bifurcations takes place in a much shorter interval of energies than in the case of the PK model. It is worth noting that in this case all the bifurcations that take place are of period doubling or symmetry breaking type, while there are no saddle-node bifurcations. We will go back to this question at the end of this section.

The first bifurcation experienced by the original NHIM is of symmetry breaking type for  $E \approx 0.01985$  a.u. In this bifurcation, two new families of unstable periodic motions (the dark blue dashed lines  $F_{01}$ ) emanate from the original unstable  $F_0$  family (the red line), that becomes a stable periodic motion for a short interval of energies. These new periodic orbits consist of two unstable off-diagonal asymmetric stretchings that migrate away from the saddle point as the energy increases without experiencing any further bifurcation, see Fig. 8(a). For an energy  $E \approx 0.0200$  a.u., the original NHIM (family  $F_0$ ) undergoes a period-doubling bifurcation in which two new families of stable periodic orbits emerge (the green lines  $F_{02}$  in Fig. 7). These new periodic motions

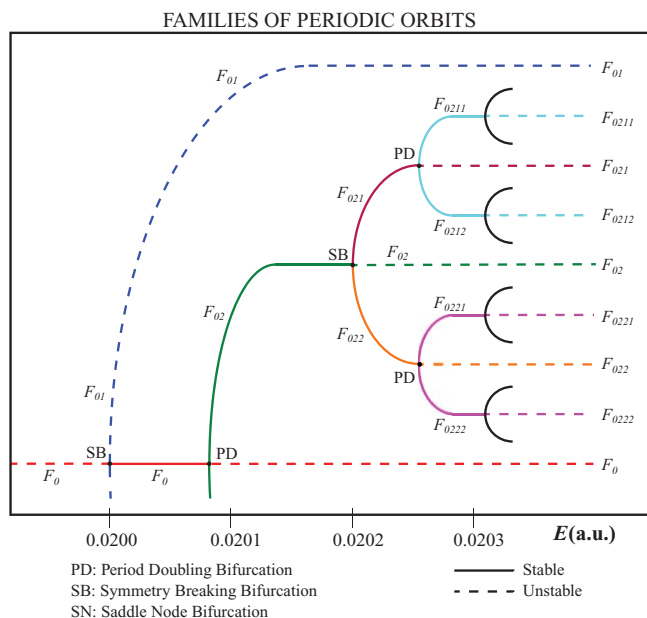


FIG. 7. Bifurcation diagram of the families of periodic orbits connected to the original NHIM ( $F_0$ ) for increasing energies  $E$  in the case of the BKMP potential energy surface.

are asymmetric stretchings with the shape of a bell centered in the diagonal of the  $(r_1, r_2)$  plane, see Fig. 8(b). As the

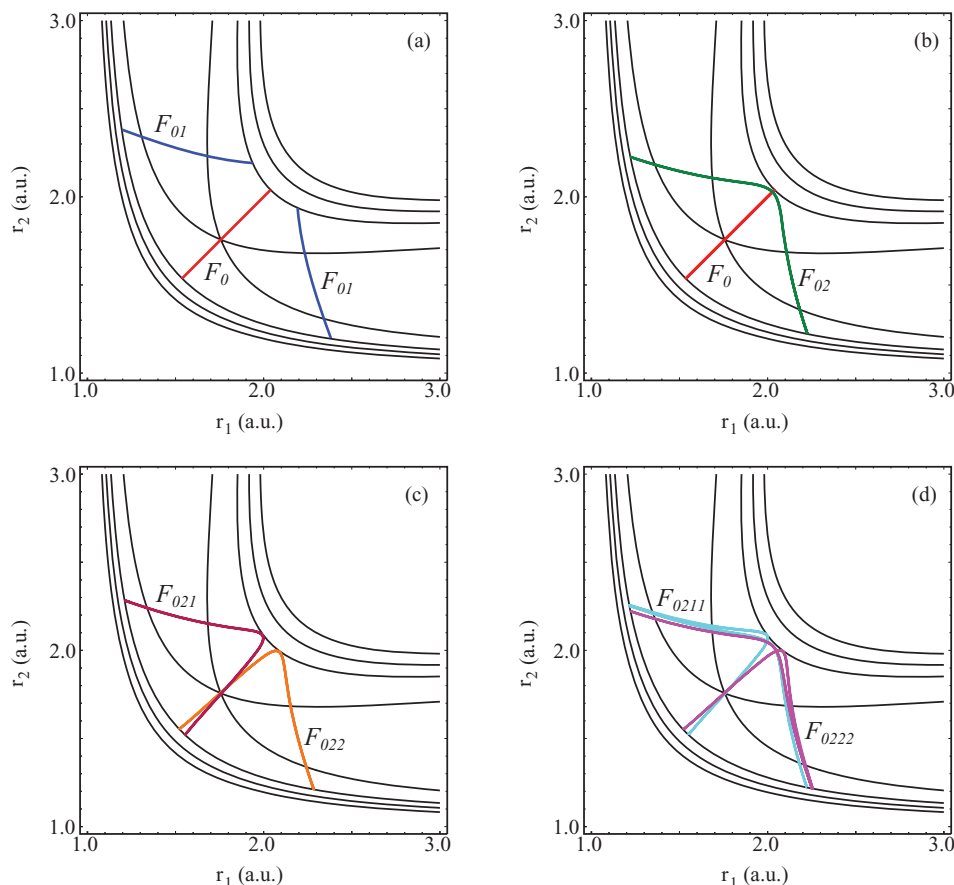


FIG. 8. Projections on the  $(r_1, r_2)$  plane of the different periodic motions involved in the bifurcations diagram of Fig. 7. In this case, all the plotted periodic motions have been calculated for an energy  $E = 0.025$  a.u. The values of the plotted equipotential lines are the saddle point energy, 0.025, 0.03, and 0.035 a.u.

energy increases, these bell shaped orbits get wider. After this bifurcation the  $F_0$  family becomes again an unstable periodic motion, without undergoing any further bifurcation for higher energies.

On the other hand, the  $F_{02}$  families undergo a symmetry breaking bifurcation for an energy  $E \approx 0.0202$  a.u. becoming unstable and two new families of stable periodic orbits appear (the orange and brown lines  $F_{021}$  and  $F_{022}$ ). These periodic motions consist of asymmetric stretchings with the shape of a bell displaced from the diagonal of the  $(r_1, r_2)$  plane, see Fig. 8(c). For higher energies, these two families experience a cascade of period-doubling bifurcations with consecutive exchanges of stability and the emergence of new families of periodic motions of increasing period. Figure 8(c) shows in the  $(r_1, r_2)$  plane the periodic orbits corresponding to the new families (the light blue and magenta lines  $F_{0211}$ ,  $F_{0212}$ ,  $F_{0221}$ , and  $F_{0222}$ ) that emanate from the first of these period-doubling bifurcations.

We already noted the big difference between the bifurcation diagrams in Figs. 5 and 7 corresponding to the PK and the BKMP potential energy surfaces. This is a surprising fact because, obviously both surfaces are built to describe the same chemical reaction. Although there are no major quantitative differences between them, as we can observe in Fig. 2 and in Table I, it is quite intriguing that, at least near the saddle point region, they provide very different descriptions of the dynamics.

However, despite the very different dynamical behavior, the reaction probability behaves essentially in the same way in both cases and it does not appear to be affected by the particular dynamics generated by the potential energy surface.

## VI. BREAKDOWN OF THE DYNAMICAL TRANSITION STATE THEORY

Li and co-workers<sup>22</sup> have studied analytically the bifurcations of the non-return transition state of the classical  $\text{H}_2 + \text{H}$  exchange reaction using the PK potential energy surface. They have performed this study by calculating the partial normal form of the system Hamiltonian in the vicinity of the saddle point. In the collinear case, these authors have detected the occurrence of two symmetric saddle-node bifurcations located at both sides of the saddle point, similarly to those we have found in this study. However, after detecting this first bifurcation, the partial normal form is unable to detect the successive bifurcations experienced by the system in a short energy range. In this way, neither the normal form nor the partial normal form can predict the complex dynamics of the system and this results in the inability to localize and/or define the existence of a non-return TS.

In order to verify this fact, we calculate the reaction probability given by the reactive flux across the unstable asymmetric stretchings  $F_1$  and  $F_{01}$  depicted by dashed blue lines in Figs. 6(a) and 8(a) (see also the bifurcation diagrams in Figs. 5 and 7). We name this reaction probability as  $P_{VTST}(E)$  because, according to variational transition state theory,<sup>2,5</sup> the periodic orbits  $F_1$  and  $F_{01}$  are transition states of minimum flux that provide an upper bound for the reaction probability. Thence, Fig. 9(a) shows the evolution of  $P_{VTST}(E)$  (the blue points), as well as the evolutions of  $P_{MC}(E)$  (the green points) and  $P_{NF}(E)$  (the red points), in the case of the PK potential energy surface. Figure 9(b) shows the evolutions of the same reaction probabilities in the case of the BKMP model.

As expected, in both potential models the evolution of the probability  $P_{VTST}(E)$  is not in agreement with the falloff predicted by  $P_{MC}(E)$  for high energies.  $P_{VTST}(E)$  presents a wrong monotonic increase, although due to the minimum flux property, it is slower than the faster growth suffered by the  $P_{NF}(E)$ . Note that for both potential models, the disagreements begin after the first bifurcation takes place: for energies  $E > 0.022$  a.u. in the PK surface and for energies  $E > 0.02$  a.u. in the BKMP one. In particular, the critical value  $E > 0.022$  a.u. for the PK surface is very similar to the energy limit value for the validity of the TST found by Sverdlik and Koepl.<sup>19</sup>

Furthermore, we have performed similar computations of  $P(E)$  with several of the new unstable periodic orbits emerging from the other bifurcations, and none of them are in agreement with  $P_{MC}(E)$ .

Therefore, these results show that, after the first bifurcation, neither the original NHIM nor any of the new unstable periodic orbits emanating from the consecutive bifurcations can be considered as the limit of a dividing surface that determines the reaction probability of the system. The origin of this behavior is that, as the energy increases, the bottleneck

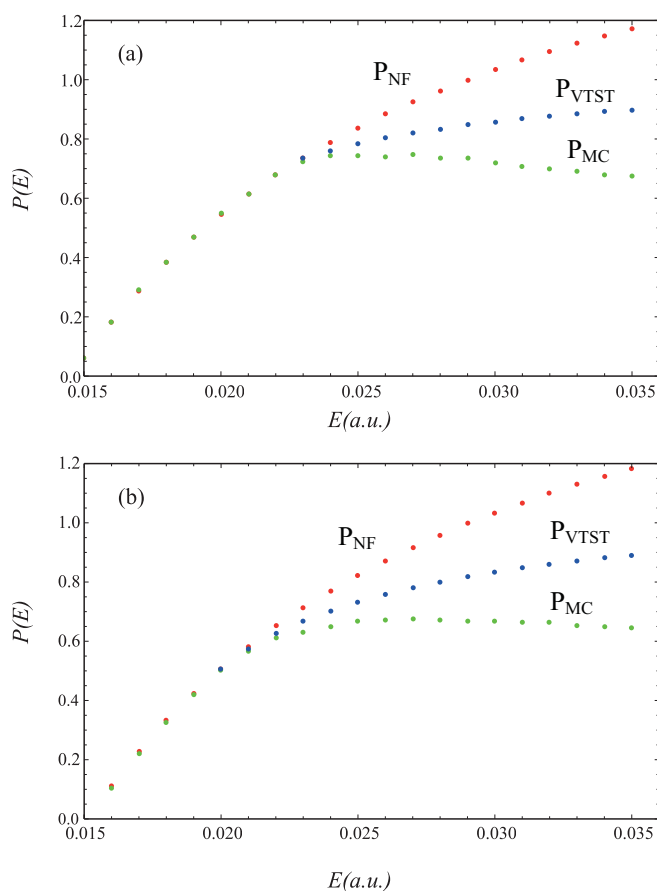


FIG. 9. Evolution of the reaction probabilities with the system energy  $E$  computed by different methods. (a) PK potential energy surface. (b) BKMP potential energy surface.

property is lost, being the cascade of bifurcations suffered by the system in the saddle region the mechanism through which this loss takes place. Then, the new periodic motions along with the original NHIM behave as multiple dynamical barriers that prevent the existence of a unique non-return transition state. Therefore, for high energies, the transition state theory suffers a sudden breakdown and it cannot be longer applied in order to compute the reaction rates.

## VII. CONCLUSIONS

In the present work we have studied the bifurcations of the unstable periodic orbit (NHIM) associated to the non-return transition state of the classical  $\text{H}_2 + \text{H}$  exchange reaction in the collinear case. We also study their effects on the evolution of the reaction probability with the system energy. In this work we have made use of two different models for the potential energy of the reaction: the classical Porter–Karplus (PK) energy surface and the more modern Boothroyd, Keogh, Martin, and Peterson (BKMP) energy surface.

We have computed the normal form of the Hamiltonian in the neighborhood of the saddle point. From the Hamiltonian normal form we have obtained explicit expressions of the dynamical structures that organize the phase space and rule the reaction: the non-return transition state, its associate NHIM

and the stable and unstable manifolds. These expressions have allowed us to visualize these four relevant dynamical structures as projections in the space of the original coordinates of the system.

We have taken advantage of the features of the NHIM in order to calculate the reaction probability as a function of the system energy in a more efficient way than with the Monte Carlo method. Under the two potential energy models considered, the evolution of the reaction probability computed with both methods are in very good agreement for low energies. Nevertheless, for higher energies in both models the reaction probability values calculated through the normal form present a wrong monotonic increase instead of the well known falloff.

This disagreement has moved us to focus on the analysis of the sequence of bifurcations suffered by the NHIM by means of the numerical continuation of the families of periodic orbits emanating from it. We found that the bifurcation diagrams calculated for both potential energy models are quite different. In the case of the PK potential energy surface, the sequence of bifurcations is quite complicate and rich and includes saddle-node, symmetry-breaking, and period-doubling bifurcations. On the other hand, in the case of the BKMP model, we detect a faster and more ordered sequence of bifurcations basically organized as a cascade of period-doubling bifurcations.

We also found that, in both potential energy models, the reaction probabilities computed by the phase flux through the NHIM and by the Monte Carlo method begin to be in disagreement when the original NHIM experiences the first bifurcation.

In order to determine if any of the new unstable periodic orbits emerging from the original NHIM replace to it in the role of defining the dividing surface, we have obtained new values of the reaction probability by calculating the phase reactive flow across these new unstable periodic orbits. For high energies, none of these new values of the reaction probability are in agreement with the behavior predicted by the Monte Carlo method. Therefore, these results show that for high energies none of the unstable periodic orbits emanating from the original NHIM can be regarded as the invariant object of the new TS ruling the reaction.

The bottleneck property can be regarded as the key in this study. For low energies the NHIM is the only one periodic orbit around the saddle point and the bottleneck property preserves. Nevertheless, as the energy increases the system begins to undergo different bifurcations in which new periodic orbits appear around the saddle. These new periodic orbits create dynamical barriers that remove the bottleneck feature. Then, they prevent the existence of a unique non-return transition state in the system. Therefore, for high energies, transition state theory is no longer valid because it is not able to

provide a unique dividing surface and then it cannot be applied to calculate the reaction probability.

## ACKNOWLEDGMENTS

This work is included in the framework of the research project MTM2008-03818 supported by the Spanish Ministry of Education and Science.

- <sup>1</sup>E. P. Wigner, *Trans. Faraday Soc.* **34**, 29 (1938); W. H. Miller, *Faraday Discuss. Chem. Soc.* **110**, 1 (1998).
- <sup>2</sup>E. Pollack and P. Pechukas, *J. Chem. Phys.* **69**, 1218 (1978).
- <sup>3</sup>E. Pollack and P. Pechukas, *J. Chem. Phys.* **70**, 325 (1979).
- <sup>4</sup>P. Pechukas and E. Pollack, *J. Chem. Phys.* **71**, 2062 (1979).
- <sup>5</sup>E. Pollack, in *The Theory of Chemical Reaction Dynamics*, edited by M. Baer, (CRC, Boca Raton, FL, 1985), Vol. 3, pp. 123–246.
- <sup>6</sup>P. Pechukas and F. H. McLafferty, *J. Chem. Phys.* **58**, 1622 (1973).
- <sup>7</sup>P. Pechukas and E. Pollack, *J. Chem. Phys.* **67**, 5976 (1977).
- <sup>8</sup>H. Waalkens and S. Wiggins *J. Phys. A* **37**, L435 (2004).
- <sup>9</sup>S. Wiggins, *Normally Hyperbolic Invariant Manifolds in Dynamical Systems* (Springer-Verlag, New York, 1994).
- <sup>10</sup>A. Deprit, *Celest. Mech.* **1**, 12 (1969); J. Palacián and P. Yanguas, *Nonlinearity* **13**, 1021 (2000).
- <sup>11</sup>T. Uzer, C. Jaffé, J. Palacián, P. Yanguas, and S. Wiggins, *Nonlinearity* **15**, 975 (2002); C. Jaffé, S. Kawai, J. Palacián, P. Yanguas, and T. Uzer, in *Geometric Structures of Phase Space in Multidimensional Chaos: Applications to Chemical Reaction Dynamics in Complex Systems*, edited by M. Toda, T. Komatsuzaki, T. Konishi, R. S. Berry, and S. A. Rice (Wiley, Hoboken, NJ, 2005), Part A, pp. 171–216; L. Wiesenfeld, *ibid.*, pp. 217–265; H. Waalkens, R. Schubert, and S. Wiggins, *Nonlinearity* **21**, R1 (2008).
- <sup>12</sup>S. Wiggins, L. Wiesenfeld, C. Jaffé, and T. Uzer, *Phys. Rev. Lett.* **86**, 5478 (2001).
- <sup>13</sup>C. Jaffé, D. Farrelly, and T. Uzer, *Phys. Rev. Lett.* **84**, 610 (2000); M. Inarrea, V. Lanchares, J. Palacián, A. I. Pascual, J. P. Salas, and P. Yanguas, *Phys. Rev. A* **76**, 052903 (2007).
- <sup>14</sup>S. D. Ross, M. W. Lo, J. Marsden, D. Farrelly, and T. Uzer, *Phys. Rev. Lett.* **89**, 011101 (2002); H. Waalkens, A. Burbanks, and S. Wiggins, *Mon. Not. R. Astron. Soc.* **361**, 763775 (2005).
- <sup>15</sup>M. J. Davis, *J. Chem. Phys.* **83**, 1016 (1985).
- <sup>16</sup>M. J. Davis and S. K. Gray, *J. Chem. Phys.* **84**, 5389 (1986).
- <sup>17</sup>M. J. Davis, *J. Chem. Phys.* **86**, 3978 (1987).
- <sup>18</sup>E. K. Grimmelmann and L. L. Lohr Jr., *Chem. Phys. Lett.* **48**, 487 (1977).
- <sup>19</sup>D. I. Sverdluk and G. W. Koeppl, *Chem. Phys. Lett.* **59**, 449 (1978).
- <sup>20</sup>I. Burghardt and P. Gaspard, *J. Chem. Phys.* **100**, 6395 (1994); *J. Phys. Chem.* **99**, 2732 (1995).
- <sup>21</sup>C. Li, A. Shoujiguchi, M. Toda, and T. Komatsuzaki, *Phys. Rev. Lett.* **97**, 028302 (2006).
- <sup>22</sup>C. Li, M. Toda, and T. Komatsuzaki, *J. Chem. Phys.* **130**, 124116 (2009).
- <sup>23</sup>H. Waalkens, A. Burbanks, and S. Wiggins, *J. Chem. Phys.* **121**, 6207 (2004).
- <sup>24</sup>R. N. Porter and M. Karplus, *J. Chem. Phys.* **40**, 1105 (1964).
- <sup>25</sup>A. I. Boothroyd, W. J. Keogh, P. G. Martin, and M. R. Peterson, *J. Chem. Phys.* **95**, 4343 (1991).
- <sup>26</sup>H. Waalkens, A. Burbanks, and S. Wiggins, *J. Phys. A* **38**, L759 (2005); *Phys. Rev. Lett.* **95**, 084301 (2005).
- <sup>27</sup>E. Doedel, R. Paffenroth, A. R. Champneys, T. F. Fairgrieve, Y. A. Kuznetsov, B. E. Oldman, B. Sandstede, and X. Wang, *AUTO 2000: Continuation and Bifurcation Software for Ordinary Differential Equations with HomCont* (Concordia University, Montreal, 2002).
- <sup>28</sup>P. Kamthan, Auto software for continuation and bifurcation problems in ordinary differential equations. See <http://indy.cs.concordia.ca/auto/>
- <sup>29</sup>F. J. Muñoz-Almaraz, E. Freire, J. Galán, E. Doedel, and A. Vanderbauwhede, *Physica D* **181**, 1 (2003).